Chinese Journal of
POLYMER SCIENCE

RESEARCH ARTICLE

https://doi.org/10.1007/s10118-024-3139-z
Chinese J. Polym. Sci.

Numerical Study of Two Opposing Weak Polyelectrolyte Brushes by the Self-consistent Field Theory

Bei-Ning Wang[a], Huan-Da Ding[b], Zhi-Kuan Chen[b], and Chao-Hui Tong[a*]

[a] *Department of Physics, Ningbo University, Ningbo 315211, China*
[b] *Ningbo Institute of Northwestern Polytechnical University, Ningbo 315103, China*

Abstract The self-consistent field theory (SCFT) was employed to numerically study the interaction and interpenetration between two opposing weak polyelectrolyte (PE) brushes formed by grafting weak PE chains onto the surfaces of two long and parallel columns with rectangular-shaped cross-section immersed in a salty aqueous solution. The dependences of the brush heights and the average degree of ionization on various system parameters were also investigated. When the brush separation is relatively large compared with the unperturbed brush height, the degree of interpenetration between the two opposing PE brushes was found to increase with increasing grafting density and bulk degree of ionization. The degree of interpenetration also increases with the bulk salt concentration in the osmotic brush regime. Numerical results further revealed that, at a brush separation comparable to the unperturbed brush height, the degree of interpenetration does not increase further with increasing bulk degree of ionization, bulk salt concentration in the osmotic regime and grafting density. The saturation of the degree of interpenetration with these system parameters indicates that the grafted PE chains in the gap between the two columns retract and tilt in order to reduce the unfavorable electrostatic and steric repulsions between the two opposing PE brushes. Based on salt ion concentrations at the midpoint between the two opposing brushes, a quantitative criterion in terms of the unperturbed brush height and Debye screening length was established to determine the threshold value of the brush separation beyond which they are truly independent from each other.

Keywords Polyelectrolyte; Polymer brush; Self-consistent field theory

Citation: Wang, B. N.; Ding, H. D.; Chen, Z. K.; Tong, C. H. Numerical study of two opposing weak polyelectrolyte brushes by the self-consistent field theory. *Chinese J. Polym. Sci.* https://doi.org/10.1007/s10118-024-3139-z

INTRODUCTION

Polyelectrolyte (PE) brushes consist of polymer chains with ionizable functional groups densely end-tethered to solid surfaces by chemical bonds or physical adsorption. When immersed in polar solvents, *e.g.*, water, the functional groups ionize and release counterions into the solvent, leading to the stretching of the grafted polymer chains normal to the grafting substrate and the formation of a swollen brush-like layer.[1–3] According to the degree of ionization of the functional groups along the chains, PE brushes can be classified into two types. The first type is the strong PE brushes in which the functional groups completely dissociate and release counterions into the polar solvent. The second type refers to the weak PE brushes in which the functional groups only partially dissociate with the degree of ionization critically governed by the physiochemical properties of the solution such as the salt concentration and the solution pH.[4,5] PE brushes can modify material surface properties and respond to a wide range of external stimuli. Thus PE brushes have found a plethora of technological applications in colloidal stabilization,[6] lubrication,[7,8] sensing and actuation,[9] smart materials,[10] nano-fluidics,[11,12] *etc*. Because of their important applications spanning so many different fields, PE brushes have attracted significant research interest.[13–39]

Over the past few years, the tribological properties of PE brushes have become a focal point of research due to their potential applications in biological lubrications.[40–48] The major human synovial joints such as hips and knees are prime examples of biological lubrications. Some bio-lubricants in these uniquely efficient tribological systems such as hyaluronan (HA) and glycoproteins are polyelectrolytes containing many sulfonic and carboxylic groups on the side chains. PE brushes are thus promising candidates for highly efficient biomimetic lubricants for artificial joints. PE brushes have been shown to be able to provide extremely efficient boundary lubrication owing to the high degree of hydration of the charged segments on the polymer backbones and the exceptional resistance to mutual interpenetration by the compressed yet swollen brush layers.[40–42] Polyelectrolyte brushes grafted onto two opposing surfaces can serve as an excellent model system for the study of lubrications of artificial joints under normal and shear forces.[21–27,33–38] Therefore, it is not surprising that the interactions between two opposing PE brushes have attracted considerable research interest. Experiments and simulations revealed a very low frictional coef-

* Corresponding author, E-mail: tongchaohui@nbu.edu.cn
Received February 20, 2024; Accepted April 7, 2024; Published online June 5, 2024

ficient when sliding one PE brush relative to the other, and showed that the frictional coefficient is directly related to the interpenetration depth of polyelectrolyte chains. Furthermore, it was found that PE brushes can support a much higher normal load than neutral brushes for the same degree of compression due to the counter-ion osmotic pressure.[8,49–57]

In the studies of the interactions and mutual interpenetration between two opposing PE brushes thus far, nearly all the theoretical and simulation studies dealt with the case of strong PE brushes.[21–27,29,50] The case of weak PE brushes has rarely been touched upon. Very recently, Duan and Chen studied the electrostatics and swelling-shrinking behaviors of two opposing strong PE brushes using a newly developed phenomenological model.[58] Distinct scaling laws of the brush height in different regimes were obtained. The anomalous shrinkage of the PE brushes with added salt was rationalized. Chen and coauthor had previous studied the electroosmotic transport in PE grafted nanochannels with pH-dependent charge density.[11,12] In this theoretical study, the degree of ionization of weak polyacid grafted onto the inner surfaces of nanochannels was explicitly taken into account. It would be interesting to extend their recent study of two opposing strong PE brushes to the case of weak PE brushes using their approach to pH-dependent charge density.

In this work, we employ a continuum self-consistent field theory (SCFT), which explicitly takes into account the acid-base ionization equilibrium, to numerically study the interaction and mutual interpenetration between two weak PE brushes formed by grafting weak polybase chains onto the surfaces of two opposing long and parallel columns with rectangular cross-sections immersed in a salty aqueous solution. Compared with molecular simulations, the SCFT offers significant computational advantages, especially for charged systems. Thus, the effects of various system parameters, such as the grafting density, the chain length, the pH of the solution, the salt concentration, and the brush separation, on the interaction and mutual interpenetration between the two weak PE brushes can be fully explored. These effects have seldomly been investigated systematically in molecular simulations. The work is organized as follows. In Section **THEORY, MODEL EQUATIONS, AND NUMERICAL METHODS**, the theory and methods used in the present work are described. Section **RESULTS AND DISCUSSION** concerning the brush height, the interaction and mutual penetration between the polyelectrolyte brushes, the average degree of ionization of the brushes, as well as the effect of the distance between two opposing PE brushes on the distributions of salt ions, are presented. In **SUMMARY AND CONCLUSIONS**, the main results are summarized.

THEORY, MODEL EQUATIONS, AND NUMERICAL METHODS

In this work, we considered a (semi)grand canonical thermodynamic system comprising weak polybase type linear polymer chains permanently and uniformly grafted on the surfaces of two long and parallel columns with rectangular cross-sections immersed in an aqueous solution with mobile point-like monovalent cations (Na^+, H^+) and anions (Cl^-, OH^-) in contact with reservoirs. A schematic diagram and a cartoon of the cross-section of the system are shown in Fig. 1(a) and Fig. 1(b), respectively.

In reality, the two opposing weak PE brushes immersed in a salty aqueous solution are three-dimensional and finite-sized objects. For simplicity and computational convenience, it was assumed that the two parallel columns are long enough such that the end effect can be neglected. Therefore, the model system can be regarded as being translationally invariant in the direction perpendicular to the cross-section of the two columns (along the axial z direction). Thus, each physical quantity can be viewed as a two-dimensional one on a per unit length in the z direction basis. The two weak PE brushes are symmetric with respect to y axis, and each brush is symmetric with respect to x axis of the system (see Fig. 1a). Here, L_x, L_y were defined as the system sizes along the x axis and y axis, respectively. We denoted the distance between the two brushes as D, the length and width of rectangle-shaped cross-sections of the substrates as L_0 and W_0, respectively. The system volume per unit length in z direction is $L_x \times L_y$. The area of the cross-section of each substrate is $S = W_0 \times L_0$. At the far left and right sides of the system along the x direction, the system is in contact with the reservoirs, in which a constant pH and salt concentration are maintained. It is noted that, for a (semi)grand canonical thermodynamic system, there is an

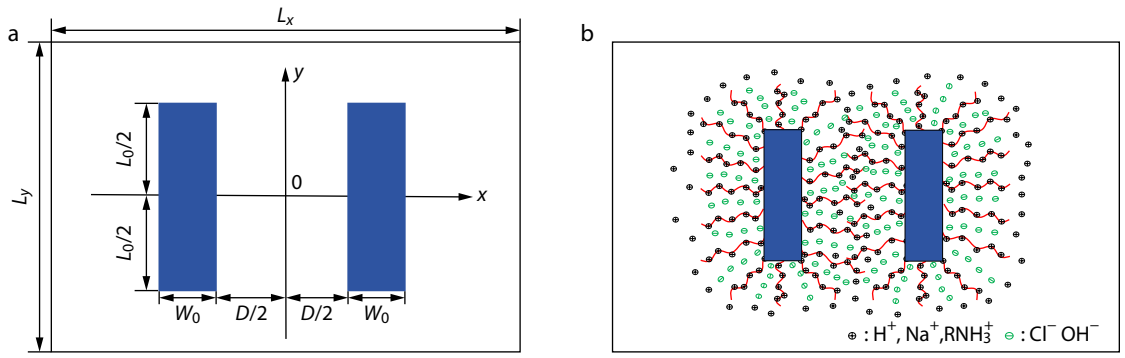

Fig. 1 (a) A schematic diagram of the rectangle-shaped cross-section of two long columns under study is displayed. The weak polybase type PE chains are grafted on the surfaces of these two columns which are immersed in an aqueous solution. The far left and right sides in the x direction are in contact with reservoirs with fixed pH and salt concentration. In the y direction, the periodic boundary condition was applied. (b) A cartoon depicting the cross-section of the system including the grafted PE chains and various types of mobile ions. Note that in the figure, the positive charges along the polymer chains correspond to RNH_3^+.

https://doi.org/10.1007/s10118-024-3139-z

inflow and outflow of particles, *e.g.*, mobile ions and solvent molecules, through the contact interface between the simulation box and the reservoir, but the inflow and outflow are in equilibrium. In the SCF equations, the Poisson-Boltzmann type equation (Eq. 8) and the modified diffusion equation (Eq. 11) are partial different equations involving the Laplacian operator, zero gradient boundary condition was applied for the electric potential and the propagators across the interface between the simulation box and the reservoirs. Along the *y* direction, the same boundary condition could also be applied. Nevertheless, in order to speed up the numerical solution of the SCF equations while retaining the important physics of our problem, the periodic condition was applied along the *y* direction. As long as the system size along the *y* direction is large enough, the two opposing brushes in the main simulation box are far apart from their periodic images. Then the periodic images will exert no influence on the interaction and interpenetration between the two opposing brushes. It was found that, compared with the boundary condition which corresponds to the two opposing PE brushes in contact with reservoirs in the *y* direction, adopting the periodic boundary condition can reduce the system size along the *y* direction by one order of magnitude in the low bulk salt concentration regime.

It was assumed that there are n_p PE chains per unit length along the *z* direction uniformly grafted onto the surfaces of the two columns. The solvent molecules and the polymer segments are of the same size with a volume $\rho_0^{-1} = a^3$. Then the grafting density which expresses the average number of grafted chains per unit surface area in the *z* direction is $\sigma_g = n_p/[4(L_0 + W_0)]$. The average volume fraction of the grafted chains is $\overline{\phi_P} = n_p N \rho_0^{-1} / \left[L_x \times L_y - 2 \times W_0 \times L_0\right]$ on a per unit length in the *z* direction basis with *N* denoting the number of monomers per PE chain.

In the self-consistent field theory for charged polymers, the multi-chain many-body problem is simplified to an effective single PE chain in a mean-field to be determined self-consistently.[5,59–61] Using the (semi)grand canonical formulation, Witte and coworkers derived the SCF equations for weak polybase brushes.[5,59] Other similar formulations which also include the acid-base chemical equilibrium, have been proposed.[62–64] According to the formulation by Witte *et al.*,[5] the dimensionless SCF equations which we used in this study are summarized as follows:

$$\omega_P\left(\vec{r}\right) = \chi_{PS} N \phi_S\left(\vec{r}\right) + \eta\left(\vec{r}\right) - N \ln\left\{1 - f_b + f_b \exp\left[-\psi\left(\vec{r}\right)\right]\right\} \quad (1)$$

$$\omega_S\left(\vec{r}\right) = \chi_{PS} N \phi_P\left(\vec{r}\right) + \eta\left(\vec{r}\right) \quad (2)$$

$$\omega_{ion}\left(\vec{r}\right) = z_{ion}\psi\left(\vec{r}\right) \quad (3)$$

$$\phi_P\left(\vec{r}\right) = \frac{\overline{\phi_P}}{Q_P}\int_0^1 \mathrm{d}s q_f\left(\vec{r}, s\right) q_g\left(\vec{r}, 1-s\right) \quad (4)$$

$$\phi_S\left(\vec{r}\right) = \phi_S^b \exp\left[\frac{\omega_S\left(x \to \pm\infty\right) - \omega_S\left(\vec{r}\right)}{N}\right] \quad (5)$$

$$\phi_{ion}\left(\vec{r}\right) = \phi_{ion}^b \exp\left[\omega_{ion}\left(x \to \pm\infty\right) - \omega_{ion}\left(\vec{r}\right)\right] \quad (6)$$

$$\phi_P\left(\vec{r}\right) + \phi_S\left(\vec{r}\right) = 1 \quad (7)$$

$$\begin{aligned}\vec{\nabla}\cdot\left[\varepsilon\left(\vec{r}\right)\vec{\nabla}\psi\left(\vec{r}\right)\right] = -N\sum\nolimits_{ion} z_{ion}\phi_{ion}\left(\vec{r}\right) - \\ N\phi_P\left(\vec{r}\right) f_b \exp\left[-\psi\left(\vec{r}\right)\right] / \left\{1 - f_b + f_b \exp\left[-\psi\left(\vec{r}\right)\right]\right\}\end{aligned} \quad (8)$$

where ϕ_j and ϕ_j^b with j = S, P, and ion are local and bulk volume fractions of solvent molecules, monomers (for PE chains, the volume-averaged density $\overline{\phi_P}$ instead of ϕ_P^b was used), and the dimensionless local and bulk number densities of point-like mobile ions (Na^+, H^+, Cl^-, OH^-), χ_{PS} denotes the Flory-Huggins interaction parameter between monomers and solvent molecules, f_b is the bulk degree of ionization or the charge fraction of PE chains in the reservoir, $\eta(\vec{r})$ is the Lagrange multiplier to enforce the incompressible condition, ω_j denotes the conjugate interaction field within the SCFT formalism, $\psi(\vec{r})$ denotes the dimensionless electric potential field $\left(\frac{e\psi}{k_B T} \to \psi\right)$, z_{ion} stand for the charge valences of the mobile ions and were set to ±1. Moreover, ε stands for the dielectric permittivity of the medium, and for simplicity, it was assumed to be the same as pure water at room temperature. Please note that, as $x \to \pm\infty$, $\psi \to 0$. In Eq. (4), the single chain partition function $Q_P = \frac{1}{V}\int \mathrm{d}\vec{r} q_f(\vec{r}, 1)$.

For the weak base type PEs studied in this work, it is straightforward to show that,

$$pK_W - pH = pK_b + \log_{10}\left[f_b/(1 - f_b)\right] \quad (9)$$

where $pK_W \equiv -\log_{10}\left(\left[H^+\right]\left[OH^-\right]\right)$ and $pK_b = -\log_{10}(K_b)$ with K_b the equilibrium constant. Thus, by adding a strong base, *e.g.*, NaOH or a strong acid, *e.g.*, HCl to the bulk solution, the pH of the bulk solution can be adjusted to afford the desired bulk charge fraction f_b. The local charge fraction of PE chains $f(\vec{r})$ is defined as:

$$f\left(\vec{r}\right) = f_b \exp\left[-\psi\left(\vec{r}\right)\right] / \left\{1 - f_b + f_b \exp\left[-\psi\left(\vec{r}\right)\right]\right\} \quad (10)$$

In Eq. (4), the propagators $q_f(\vec{r}, s)$ and $q_g(\vec{r}, s)$ denote the probability distribution function of the end-segment of a polymer chain of length s at $\vec{r}$ with one end (q_f (s=0)) free and the other end (q_g (s=0)) grafted onto the substrate, respectively. They both satisfy the following modified diffusion equation:

$$\frac{\partial q\left(\vec{r}, s\right)}{\partial s} = \nabla^2 q\left(\vec{r}, s\right) - \omega_P\left(\vec{r}\right) q\left(\vec{r}, s\right) \quad (11)$$

We applied the same boundary conditions and initial conditions for $q_f(\vec{r}, s)$ and $q_g(\vec{r}, s)$ as those proposed by Kim and Masten for polymer brushes with a fixed uniform grafting density on the surface of the grafting substrate.[65] For the present study, the Dirichlet boundary condition was applied on the surface of the grafting substrates with $q_f(\vec{r}, s) = 0$, $q_g(\vec{r}, s) = 0$. The initial condition for $q_f(\vec{r}, s)$ is $q_f(\vec{r}, s = 0) = 1$ at all computational grids except the surface grids on the substrates. At the first layer of the computational grids away from the surface of the grafting substrates, $q_g(s = 0)$ equals the inverse of $q_f(s = 1)$ at the same grids, while $q_g(s = 0)$ equals zero at all other grids.

The density profile of the PE brushes was examined in the study. Due to the symmetry, we only considered the left

brush which was formed by grafting PE chains on the surface of the left column. Using the propagators of the grafted PE chains, we can obtain the density profile of the left brush as follows:

$$\phi_{\mathrm{P}}^{\mathrm{L}}\left(\vec{r}\right)=\frac{\overline{\phi_{\mathrm{P}}}}{2Q_{\mathrm{P}}}\int_0^1 \mathrm{d}s q_{\mathrm{f}}\left(\vec{r},s\right)q_{\mathrm{g}}\left(\vec{r},1-s\right) \tag{12}$$

The boundary conditions and initial conditions in numerically solving Eq. (11) to obtain $q_{\mathrm{f}}\left(\vec{r},s\right)$ and $q_{\mathrm{g}}\left(\vec{r},s\right)$ in Eq. (12) are the same as those outlined in the preceding paragraph. Note that $q_{\mathrm{g}}\left(\vec{r},s\right)$ in Eq. (12) is only related to the left column.

The monomer density profiles of the PE chains grafted on the left and right surfaces of the left column were obtained similarly using the following expression:

$$\phi_{\mathrm{P}}^{\mathrm{LL}}\left(\vec{r}\right)=\phi_{\mathrm{P}}^{\mathrm{LR}}\left(\vec{r}\right)=\frac{L_0}{4\left(L_0+W_0\right)}\frac{\overline{\phi_{\mathrm{P}}}}{Q_{\mathrm{P}}}\int_0^1 \mathrm{d}s q_{\mathrm{f}}\left(\vec{r},s\right)q_{\mathrm{g}}\left(\vec{r},1-s\right) \tag{13}$$

Also, please note that $q_{\mathrm{g}}\left(\vec{r},s\right)$ in the above equation are only related to the left and right surfaces of the left column, respectively. $\phi_{\mathrm{P}}^{\mathrm{LL}}$ was used to compute the brush height H_{L} of the left surface of the left brush. The brush height can be calculated through the following equation:

$$H_{\mathrm{L}}^2=\frac{\int_{-L_0/2}^{L_0/2}\mathrm{d}y\int_{-L_x/2}^{-W_0-D/2}\mathrm{d}x\phi_{\mathrm{P}}^{\mathrm{LL}}\left(x,y\right)\times\left(-x-W_0-\frac{D}{2}\right)^2}{\int_{-L_0/2}^{L_0/2}\mathrm{d}y\int_{-L_x/2}^{-W_0-D/2}\mathrm{d}x\phi_{\mathrm{P}}^{\mathrm{LL}}\left(x,y\right)} \tag{14}$$

The expressions for other surface brush heights have similar forms. H_{R}, H_{T} represent the brush height of the right surface, the top surface of the left brush, respectively. By symmetry, the brush height of the bottom surface of the left brush is the same as that of the top surface.

$\phi_{\mathrm{P}}^{\mathrm{LR}}\left(\vec{r}\right)$ was used to compute the degree of interpenetration D_{I} between the left and right brushes which is defined as follows:

$$D_{\mathrm{I}}=\int_{-L_0/2}^{L_0/2}\mathrm{d}y\int_0^{D/2}\mathrm{d}x\phi_{\mathrm{P}}^{\mathrm{LR}}\left(x,y\right)/\int_{-L_0/2}^{L_0/2}\mathrm{d}y\int_{-D/2}^{D/2}\mathrm{d}x\phi_{\mathrm{P}}^{\mathrm{LR}}\left(x,y\right) \tag{15}$$

The average degree of ionization of the monomers along the polymer chains grafted on the left or right surfaces of the left column can be computed as follows:

$$\overline{f_{\mathrm{L}}}=\int f\left(\vec{r}\right)\phi_{\mathrm{P}}^{\mathrm{LL}}\left(\vec{r}\right)\mathrm{d}\,\vec{r}\,/\int\phi_{\mathrm{P}}^{\mathrm{LL}}\left(\vec{r}\right)\mathrm{d}\,\vec{r} \tag{16}$$

RESULTS AND DISCUSSION

In this study, the input parameters for the SCFT numerical studies are listed in Table 1. The radius of gyration of a PE chain R_{g} was used to non-dimensionalize the SCFT equations for the current weakly charged and flexible PE system. The monomer size a was set to 0.7 nm, which is identical to the Bjerrum length in water at room temperature. With such a monomer size, the charge fraction or the average charge in units of e carried by one monomer can approach 1 and the phenomenon of counterion condensation can be disregarded.[66] The chain length was fixed as N=50. Thus $R_{\mathrm{g}}\equiv a\sqrt{N/6}\approx 2.89a$. The dimensionless grafting density which is equal to $\sigma_{\mathrm{g}}a^2$ was varied from 0.05 to 0.3. The dimensionless NaCl salt concentration in the reservoir $C_{\mathrm{S}}^{\mathrm{b}}$ is defined as the product of the number density of Cl^- ions in the reservoir in units of m^{-3} and a^3 (the volume of one monomer). It was adjusted from $C_{\mathrm{S}}^{\mathrm{b}}=2.1\times10^{-6}$ to $C_{\mathrm{S}}^{\mathrm{b}}=3.2\times10^{-2}$, which corresponds to a bulk salt molar concentration of 1.0×10^{-5} mol/L to 0.15 mol/L. Please note that for the present polybase brush system, $\phi_{\mathrm{Na^+}}^{b}=C_{\mathrm{S}}^{\mathrm{b}}+\phi_{\mathrm{OH^-}}^{\mathrm{b}}-\phi_{\mathrm{H^+}}^{\mathrm{b}}$ and $\phi_{\mathrm{Cl^-}}^{\mathrm{b}}=C_{\mathrm{S}}^{\mathrm{b}}$, so that the condition of charge neutrality inside the reservoir is maintained. The bulk monomer charge fraction was varied from 0.05 to 0.4, which corresponds to pH values of 10.28 to 9.18 inside the reservoir. In Table 1, the dimensionless dielectric permittivity $\varepsilon=6\varepsilon_0\varepsilon_{\mathrm{s}}ak_{\mathrm{B}}T/e^2$ with ε_0 and ε_{s} denoting the vacuum permittivity and the dielectric constant of the system, respectively. In the expression, e denotes an elementary charge. ε=0.476 corresponds to ε_{s}=78.0 which is the dielectric constant of water at room temperature. The system size along the x direction L_x was varied from $256R_{\mathrm{g}}$ at low bulk salt concentration to $64R_{\mathrm{g}}$ at high bulk salt concentration. The system size along the y direction L_y was fixed at $32R_{\mathrm{g}}$. At $32R_{\mathrm{g}}$, the separation between the two opposing brushes in our simulation box and their periodic images along the y direction is $24R_{\mathrm{g}}$. Further increasing of the system size L_y was found to have no effect on the physical characteristics investigated in this study such as the degree of interpenetration, the brush height and the average degree of ionization.

Table 1 Input parameters for the SCFT numerical studies.

Monomer size (a)	0.7 nm
Chain length (N)	50
Flory-Huggins parameter (χ_{PS})	0.0
Dimensionless grafting density (σ_{g})	0.05–0.3
Dimension of the cross section ($W_0\times L_0$)	$2\times8R_{\mathrm{g}}$
Bulk monomer charge fraction (f_{b})	0.05-0.4
Dimensionless dielectric permittivity (ε)	0.4726
Separation between the two brushes (D)	$4R_{\mathrm{g}}$–$48R_{\mathrm{g}}$
Acid-base ionization constant (K_{b})	10^{-5}
Dimensionless bulk salt concentration (C_S^b)	2.1×10^{-6}–3.2×10^{-2}

The Interaction and the Degree of Interpenetration between the Two Opposing Weak PE Brushes

We systematically examined the variation of the degree of interpenetration of the two opposing weak PE brushes with the distance of separation between them. A typical example is shown in Fig. 2. As expected, the degree of interpenetration between the two opposing brushes increases with decreasing brush separation after the onset of direction interaction between them. For the systems corresponding to Fig. 2, it was found from the SCFT calculations that the brush heights of both the left and right brushes on the left column remain unchanged if the separation between the two columns exceeds about $16R_{\mathrm{g}}$. Such a brush height corresponding to two nearly independent brushes will hereinafter be called an unperturbed brush height. The unperturbed brush heights are about 5.7 and $6.4R_{\mathrm{g}}$ at $C_{\mathrm{S}}^{\mathrm{b}}=2.1\times10^{-6}$ and $C_{\mathrm{S}}^{\mathrm{b}}=2.1\times10^{-2}$, respectively (see Fig. 3). The two curves corresponding to high and low bulk salt concentrations shown in Fig. 2 nearly overlap with each other except in the low degree of interpenetration regime. The apparent difference in D_{I} in the low degree of interpenetration regime is presumably due to the larger brush height at higher bulk salt concentration.

Two-dimensional contour plots of the monomer density in

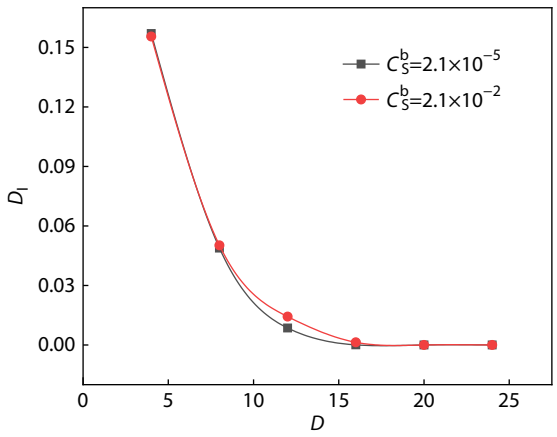

Fig. 2 Plots of the dependence of the degree of interpenetration D_I on the distance between the two PE brushes at two different bulk salt concentrations. The other system parameters are f_b=0.4, σ_g=0.1. Note that D is in units of R_g in the figure.

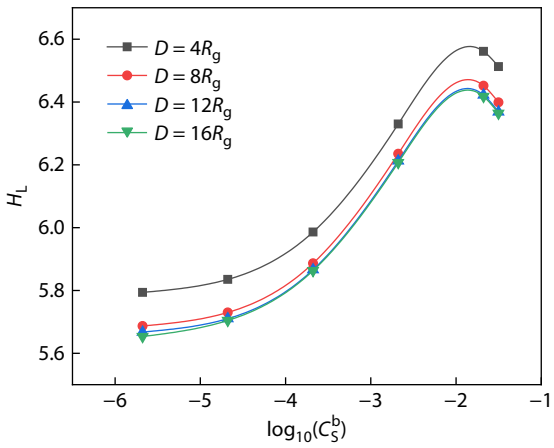

Fig. 3 The brush heights of the left surface (see definition in Eq. 14) are plotted against the bulk salt concentration at different brush separations. The other system parameters are f_b=0.4, σ_g=0.1. Note the brush height is in units of R_g.

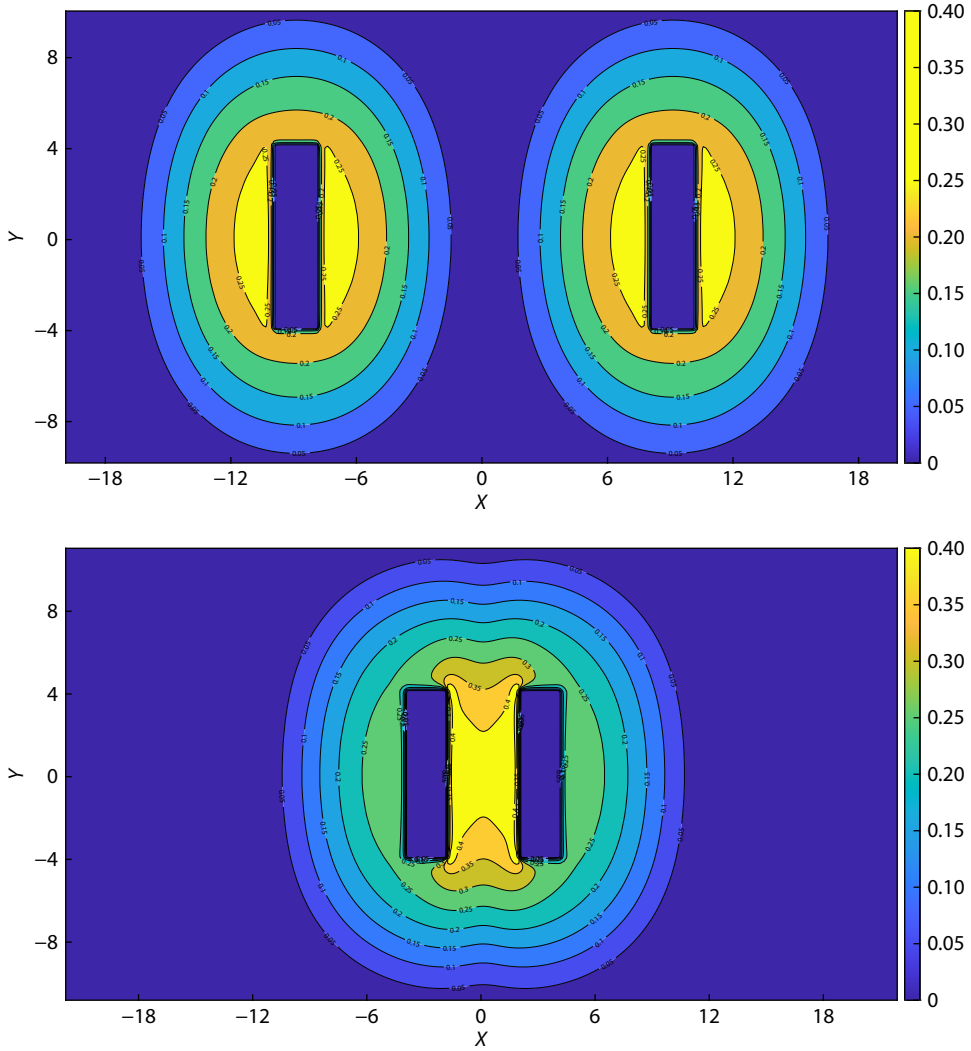

Fig. 4 The 2D contour plots of the monomer density of two opposing weak PE brushes at two different brush separations (D = 16R_g and 4R_g for the top and bottom figures, respectively). The other system parameters are f_b=0.4, σ_g=0.1, C_S^b = 2.1 × 10^{-2}. The scales for both x and y axes are in units of R_g. The total lengths of the system in the x and y directions are 64R_g and 32R_g, respectively.

https://doi.org/10.1007/s10118-024-3139-z

the system at a large and a very small brush separation are shown in Fig. 4, indicating two nearly independent and two strongly interacting brushes, respectively. This numerical result suggests that, in the regime where the brush separation is greater than about three times the unperturbed brush height, *i.e.*, $D > 3H$, the two PE brushes are well-separated and independent from each other. In the regime of $D < 3H$, the two PE brushes are interacting with each other which results in compression and interpenetration of the two brushes. As shown in Fig. 2, the degree of interpenetration is about 0.16 at a brush separation of $4R_g$. Noting that the unperturbed brush height is about $6R_g$, such a low value of degree of interpenetration at a brush separation of $4R_g$ demonstrates unequivocally that the compression and retraction of weak PE brushes is more dominant than the mutual interpenetration when two opposing brushes are brought into close contact. Indeed, as can be seen from Fig. 5, the brush height of the right surface of the left brush is only about $2.8R_g$ at $D = 4R_g$. Such a phenomenon was also observed in the case of two opposing strong PE brushes in our previous SCFT study, as well as in experiments.[54,67] In the rest of the paper, when referring to the left surface and/or right surface of the left brush, the phrase of "the left brush" will be omitted.

Apart from the bulk salt concentration, the grafting density σ_g and the bulk degree of ionization f_b are two important parameters that could affect the degree of interpenetration of two opposing weak PE brushes. As shown in Fig. 6, the degree of interpenetration increases with increasing grafting density. This is due to the fact that a higher grafting density leads to a higher degree of crowdedness and stronger steric repulsion among neighboring grafted chains. Thus, the unperturbed brush height increases with increasing grafting density. On the other hand, compared with the grafting density, the bulk degree of ionization exerts a much weaker influence on the degree of interpenetration as illustrated in Fig. 7.

The Behaviors of the Brush Height, the Average Degree of Ionization of Two Opposing Weak PE Brushes

The dependence of the brush heights of the left and right surfaces on various system parameters

The effect of the bulk salt concentration on the height of the weak PE chains grafted on the left surface is shown in Fig. 3. Two regimes, *i.e.*, the osmotic brush and the salty brush regimes, respectively, can be clearly identified from Fig. 3. In the so-called osmotic brush regime, the brush height increases with increasing bulk salt concentration. This is because the local degree of ionization of weak PE chains is enhanced due to the suppressing of the local electric potential with added salt ions. On the other hand, in the salty brush regime, the salt concentration gets sufficiently high such that the electrostatic screening effect of mobile salt ions becomes predominant, although the weak PE chains are fully ionized under such high salt concentration condition. Therefore, the height of weak PE brushes decreases with increasing salt concentration in the salty brush regime. It can be also seen from Fig. 3 that, as the two opposing brushes are brought closer to each other, the curve of brush height versus bulk salt concentration shifts slightly upwards. It is noted that when the two opposing brushes are brought together, the PE chains grafted on the opposing surfaces (interior surfaces) of the two columns can escape from the gap between the two columns by a simple lateral displacement or tilting, thus squeezing and pushing the PE chains grafted on the exterior surfaces of the two columns together, resulting in an increase in the

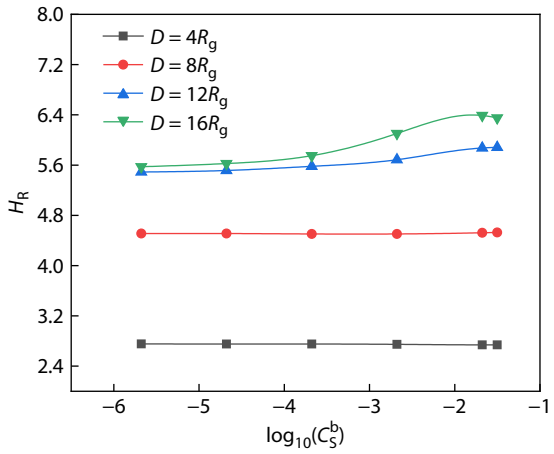

Fig. 5 The brush heights of the right surface are plotted against the bulk salt concentration at different brush separations. The other system parameters are f_b=0.4, σ_g=0.1.

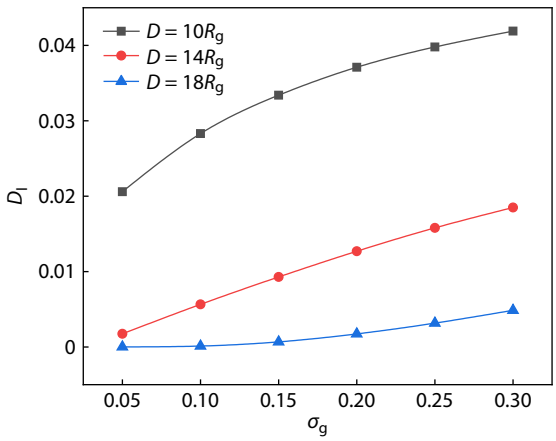

Fig. 6 Variation of the degree of interpenetration D_I with the grafting density of PE brushes at three different brush separations. The system parameters are f_b=0.4, $C_S^b = 2.1\times10^{-2}$.

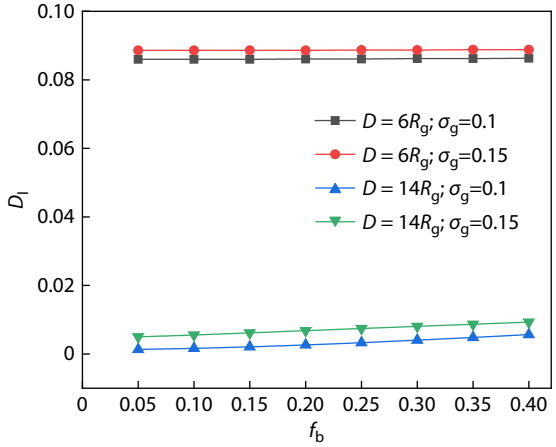

Fig. 7 Variation of the degree of interpenetration D_I with the bulk degree of ionization at different grafting densities and brush separations. In the systems $C_S^b = 2.1\times10^{-2}$.

https://doi.org/10.1007/s10118-024-3139-z

brush height of the left surface. On the contrary, as shown in Fig. 5, when the separation between the two opposing brushes is small, the bulk salt concentration has no effect on the height of the PE chains grafted on the opposing (interior) surfaces of the two columns. This result is consistent with the non-dependence of the degree of interpenetration on the bulk salt concentration at small separation between the two opposing brushes shown in Fig. 2. Furthermore, the downward shift of the curves with decreasing separation between the two opposing brushes shown in Fig. 5 demonstrates that the grafted chains in the gap between the two columns shrink and retract when the two columns are brought closer together.

The brush height of the left surface increases slightly with increasing bulk degree of ionization in an almost linear fashion as shown in Fig. 8. In the inset of Fig. 8, the brush height of the left surface is plotted as a function of the grafting density, which shows that compared with the bulk degree of ionization, the grafting density exerts a stronger influence on the brush height. On the other hand, as shown in Fig. 9, when the two opposing brushes are at the same distance of separation as that in Fig. 8, the brush height of the right surface is almost irrespective of the bulk degree of ionization. When the two opposing brushes are relatively farther apart, *e.g.*, D = $14R_g$, as shown in the inset of Fig. 9, the brush height of the right surface increases with increasing grafting density, but eventually levels off at high grafting density. In the high grafting density regime, the grafted PE chains in the gap between the two columns are strongly stretched which would lead to a higher degree of interpenetration between the two opposing brushes. These chains in the gap would retract and tilt to avoid strong interpenetration, resulting in the level off the brush height of the right surface in the high grafting density regime.

The dependence of the average degree of ionization of the left brush on various system parameters

The average degrees of ionization of the weak PE chains grafted on the left and right surfaces of the left column were investigated. It can be clearly seen from Figs. 10 and 11 that the average

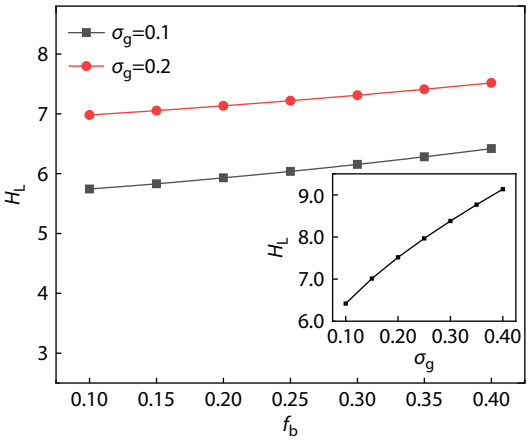

Fig. 8 The brush heights of the left surface are plotted against the bulk degree of ionization at two different grafting densities. The other system parameters are D = $14R_g$, $C_S^b = 2.1\times10^{-2}$. In the inset, the brush height of the left surface of the left brush is plotted against the grafting density. The other system parameters are D = $14R_g$, $C_S^b = 2.1\times10^{-2}$, f_b=0.4.

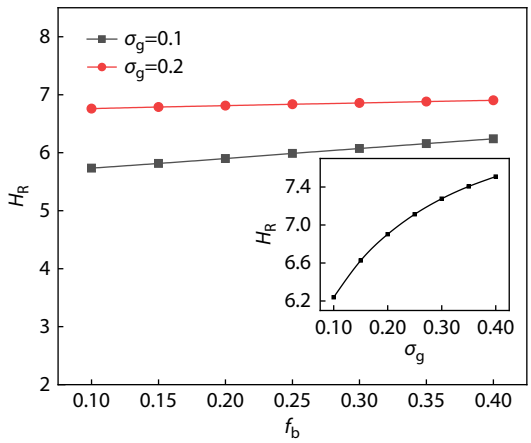

Fig. 9 The brush heights of the right surface are plotted against the bulk degree of ionization at two different grafting densities. The other system parameters are D = $14R_g$, $C_S^b = 2.1\times10^{-2}$. In the inset, the brush height of the right surface of the left brush is plotted against the grafting density. The other system parameters are D = $14R_g$, $C_S^b = 2.1\times10^{-2}$, f_b=0.4.

degrees of ionization of the weak PE chains grafted on both the left and right surfaces increase in a linear fashion with the bulk degree of ionization, and the average degree of ionization of the weak PE chains on the left surface is slightly higher than that of PE chains on the right surface. As shown in the insets of Figs. 10 and 11, the average degree of ionization decreases with increasing grafting density. The local degree of ionization is an increasing function of the bulk salt concentration as illustrated in Fig. 12. Then the average degree of ionization is also an increasing function of the bulk salt concentration as shown in Fig. 13. As the two opposing weak PE brushes are brought closer to each other, the average degree of ionization of the PE chains grafted on the right surface slightly decreases as illustrated in Fig. 13. On the other hand, the average degree of ionization of the PE chains grafted on the left surface is not affected when the two

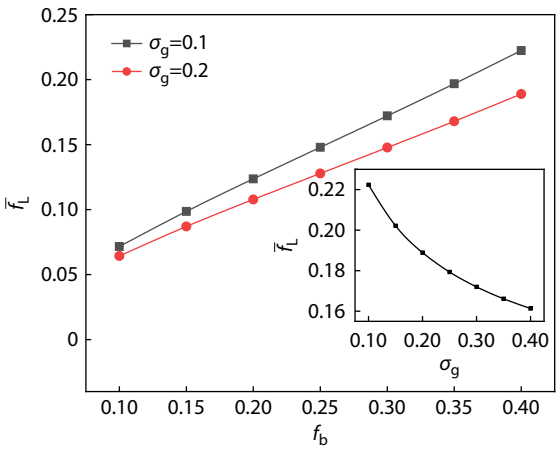

Fig. 10 The average degrees of ionization of the PE chains grafted on the left surface as a function of the bulk degree of ionization at two different grafting densities are displayed. The other system parameters are D = $14R_g$, $C_S^b = 2.1\times10^{-2}$. In the inset, the average degree of ionization of the PE chains grafted on the left surface as a function of the grafting density is shown. The other system parameters are D = $14R_g$, $C_S^b = 2.1\times10^{-2}$, f_b=0.4.

https://doi.org/10.1007/s10118-024-3139-z

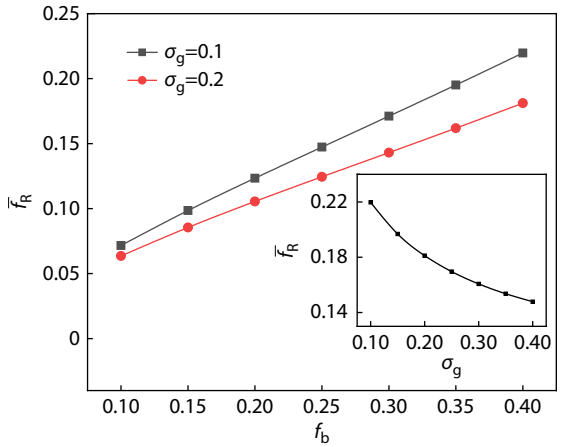

Fig. 11 The average degrees of ionization of the PE chains grafted on the right surface as a function of the bulk degree of ionization at two different grafting densities are displayed. The other system parameters are the same as those in Fig. 10. In the inset, the average degree of ionization of the PE chains grafted on the left surface as a function of the grafting density is shown. The other system parameters are the same as those corresponding to the curve in the inset of Fig. 10.

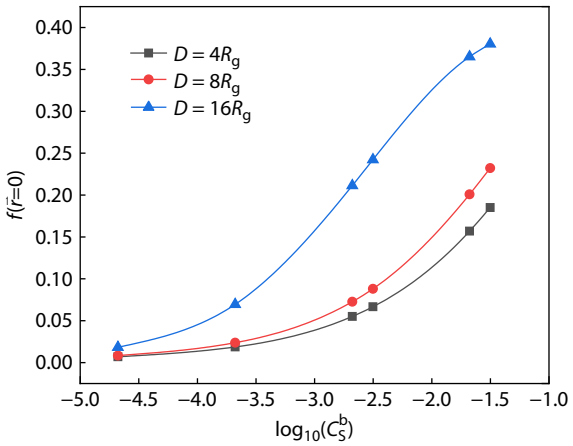

Fig. 12 The local degrees of ionization of the weak PE brushes at the center of the simulation box as a function of the bulk salt concentration at different brush separations are displayed. The other system parameters are f_b=0.4, σ_g=0.1.

opposing brushes approach each other.

Effect of the Distance between the Two Opposing Brushes on the Distributions of Salt Ions

Because the monomers of the weak polybase type brushes are positive charged, Na^+ ions should be deleted from the brush region, while Cl^- ions should be enriched inside the brush region. As shown in Figs. 14 and 15, at large brush separation, *e.g.*, $D = 20R_g$, the distributions of salt ions along the *x* axis are symmetric with respect to each column. Na^+ ions are depleted and Cl^- are enriched near the left and right surfaces of each column on which polymer chains are grafted. As the two opposing brushes approach each other, the distributions of salt ions in the exterior region of the two brushes remain unchanged. On the other hand, it can be clearly seen from Figs. 14 and 15 that the Na^+ ion concentration in the interior region decreases with decreasing brush separation. The opposite trend was found for Cl^- ion. Such

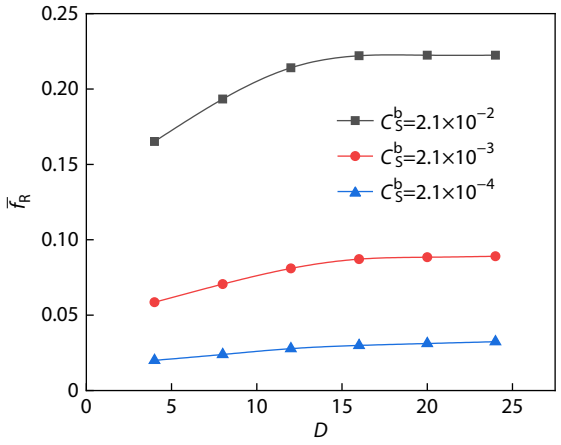

Fig. 13 The average degrees of ionization of the PE chains grafted on the right surface as a function of the brush separation at three different bulk salt concentrations are displayed. The other system parameters are f_b=0.4, σ_g=0.1.

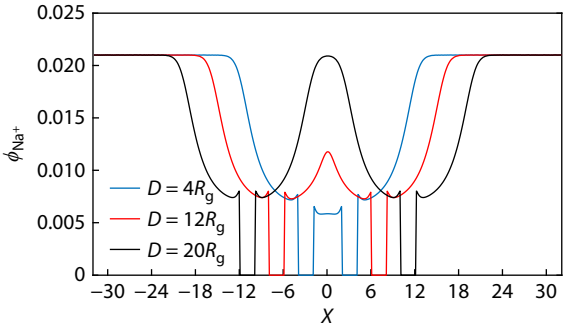

Fig. 14 The density distributions of Na^+ along the *x* axis at different brush separations are displayed. The other system parameters are f_b=0.4, σ_g=0.1, $C_S^b = 2.1\times10^{-2}$.

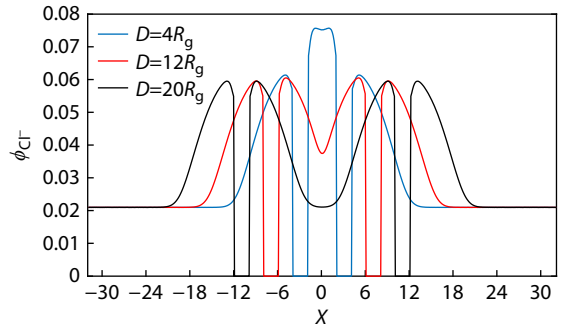

Fig. 15 The density distributions of Cl^- along the *x* axis at different brush separations are displayed. The other system parameters are f_b=0.4, σ_g=0.1, $C_S^b = 2.1\times10^{-2}$.

opposite trends of Na^+ and Cl^- ions in the interior region are due to the fact that, as the two brushes approach each other, the monomer concentration in the interior region gets higher. Although the average degree of ionization of the monomers in the interior region becomes slightly lower with decreasing brush separation (see Fig. 13), the monomer charge density still gets higher as the two opposing brushes approach each other. Therefore, a higher Cl^- concentration is entailed to neutralize the positive charges on the monomers in the interior region between the two brushes.

https://doi.org/10.1007/s10118-024-3139-z

In sub-section **The Interaction and the Degree of Interpenetration between the Two Opposing Weak PE Brushes**, from the dependence of the degree of interpenetration between the two opposing brushes on the distance between them, it was speculated that, in the regime where the brush separation is greater than about three times the unperturbed brush height, *i.e.*, $D > 3H$, the two PE brushes are well-separated and independent from each other. However, a careful examination of salt ion distributions along the x axis revealed that the concentrations of both Na^+ and Cl^- at the origin of the x axis are critically governed by both brush separation and bulk salt concentration. If the two opposing PE brushes are truly independent from each other, salt ion concentrations at the midpoint between them, *i.e.*, the origin of the x axis, should the same as the bulk values. It can be clearly seen from Figs. 14, 16 and 17 that the critical distance between the two opposing brushes, beyond which Na^+ ion concentration at the origin is equal to the bulk concentration, increases with decreasing bulk salt concentration. At $C_S^b = 2.1\times10^{-4}$ as shown in Fig. 17, the two opposing brushes should be independent from each other if the brush separation exceeds about $50R_g$. Apparently, the electrostatic screening effect of salt ions is very important in determining the threshold value of the brush separation beyond which the two opposing brushes are truly independent from each other.

The strength of the electrostatic screening effect of mobile ions in an aqueous solution can be quantified by the Debye screening length λ which is defined as $\lambda = \left(4\pi l_B \sum_i n_i\right)^{-1/2}$. In this expression, l_B denotes the Bjerrum length which is about 7×10^{-10} m, n_i refers to the number density in units of m^{-3} of ion species i. At bulk salt concentrations of $C_S^b = 2.1\times10^{-2}$, $C_S^b = 2.1\times10^{-3}$ and $C_S^b = 2.1\times10^{-4}$, which correspond to molar concentrations of 0.1, 0.01 and 0.001 mol/L, the Debye screening lengths are 1.0, 3.1 and 10.0 nm, respectively. In the present study, $1R_g \approx 2$ nm. Please note that in Figs. 14–17, f_b=0.4, which corresponds to a pH of 9.18. Then the molar concentration of OH^- is about 10^{-5} mol/L. Therefore, its contribution to the Debye screening length can be neglected.

Because of the electrostatic screening of surrounding mobile ions, the electric potential at a distance of r due to a point charge changes $\frac{Q}{4\pi\varepsilon r} \rightarrow \frac{Qe^{-r/\lambda}}{4\pi\varepsilon r}$. Then the electrostatic effect caused by a source point charge in a salty aqueous solution

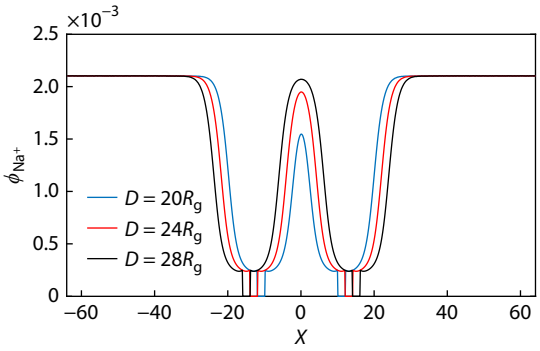

Fig. 16 The density distributions of Na^+ along the x axis at different brush separations are displayed. The other system parameters are f_b=0.4, σ_g=0.1, $C_S^b = 2.1\times10^{-3}$.

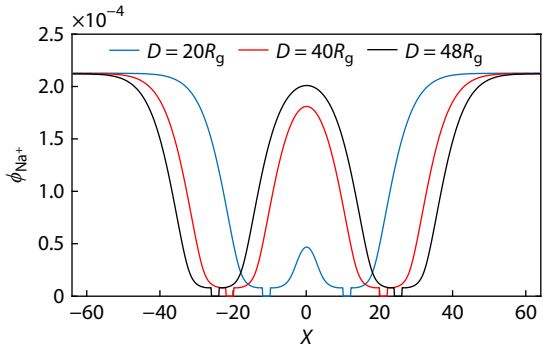

Fig. 17 The density distributions of Na^+ along the x axis at different brush separations are displayed. The other system parameters are f_b=0.4, σ_g=0.1, $C_S^b = 2.1\times10^{-4}$.

can be neglected if the distance from the source charge exceeds about 3 times the Debye screening length. Therefore, it can be conjectured that if the brush separation between two opposing PE brushes $D > 3H + 6\lambda$, they should be independent from each other. Using $H \approx 6R_g$ as shown in Fig. 3 and $\lambda = 0.5R_g, 1.6R_g, 5.0R_g$ at $C_S^b = 2.1\times10^{-2}$, $C_S^b = 2.1\times10^{-3}$ and $C_S^b = 2.1\times10^{-4}$, the threshold values of the brush separation beyond which two opposing PE brushes are independent from other were found to be $21R_g$, $28R_g$ and $48R_g$ for the systems corresponding to Figs. 14, 16 and 17, respectively. Indeed, the proposed formula of $D > 3H + 6\lambda$ for the brush separation agrees with the numerical results shown in Figs. 14, 16 and 17 quite well.

SUMMARY AND CONCLUSIONS

In this study, the self-consistent field theory was employed to numerically study the interaction and interpenetration between two opposing weak polyelectrolyte (PE) brushes immersed in a salty aqueous solution. The dependences of the brush heights and the average degree of ionization on various system parameters were also investigated.

The numerical study revealed different dependences of the degree of interpenetration on system parameters at different brushes separations. When the brush separation is relatively large compared with the unperturbed brush height, the degree of interpenetration between the two opposing PE brushes was found to increase with increasing grafting density and bulk degree of ionization. The degree of interpenetration also increases with the bulk salt concentration in the osmotic brush regime. Such increasing trend of the degree of interpenetration is due to fact that the brush height increases with these system parameters. Numerical results further showed that, at a brush separation comparable to the brush height, the degree of interpenetration does not increase further with increasing bulk degree of ionization, bulk salt concentration in the osmotic regime and grafting density. The saturation of the degree of interpenetration with these system parameters indicates that PE brushes shrink, retract and tilt in order to reduce unfavorable electrostatic and steric repulsions between the two PE brushes. Such a saturation of the degree of interpenetration has also been observed for two opposing strong PE brushes.[68] The numerical SCFT study in this work demon-

https://doi.org/10.1007/s10118-024-3139-z

strates unequivocally that the compression and retraction of PE brushes is more dominant than the mutual interpenetration for two opposing PE brushes.

In this study, the threshold value of the brush separation between two opposing PE brushes beyond which they are truly independent from each other was critically examined. It was found that the parameter of degree of interpenetration is insensitive to change of bulk salt concentration and thus is unable to respond to the electrostatic screening effect of mobile ions. On the contrary, salt ion distributions in the gap between the two grafting substrates are very sensitive to changes of brush separation and bulk salt concentration. Based on salt ion concentrations at the midpoint between the two brushes, a quantitative criterion in terms of the unperturbed brush height and Debye screening length was established to determine the threshold value of the brush separation between two opposing PE brushes beyond which they are truly independent from each other. Such a criterion was found to agree with the numerical results quite well.

As shown in previous studies, the fluidity of the hydration shells surrounding the charged segments of PE brushes contributes significantly to the extremely low frictional forces between charged polymer brushes. As a coarse-grained mean-field theory, SCFT treats water as a continuum dielectric background. Thus, the hydration of charged species and the effect of water on the lubrication between opposing PE brushes were completely ignored in the SCFT. These issues can be much better tackled with the Atomistic Molecular Dynamics simulations, although much more computationally demanding.

Conflict of Interests

The authors declare no interest conflict.

Data Availability Statement

The related data (DOI:10.57760/sciencedb.j00189.00018) of this paper can be accessed in the Science Date Bank database https://www.scidb.cn/en/c/cjps.

ACKNOWLEDGMENTS

This work was financially supported by the National Natural Science Foundation of China (No. 21774067) and The Foundation of Key Laboratory of Flexible Electronics of Zhejiang Province (No. 2023FE004). C. T. acknowledges the support from K. C. Wong Magna at Ningbo University.

REFERENCES

1 Halperin, A.; Tirrell, M.; Lodge, T. P. Tethered chains in polymer microstructures. *Adv. Polym. Sci.* **1991**, *100*, 30–71.
2 Rühe, J.; Ballauff, M.; Biesalski, M.; Dziezok, P.; Gröhn, F.; Johannsmann, D. Polyelectrolyte brushes. *Adv. Polym. Sci.* **2004**, *165*, 79–150.
3 Naji, A.; Seidel, C.; Netz, R. R. Theoretical approaches to neutral and charged polymer brushes. *Adv. Polym. Sci.* **2006**, *198*, DOI:10.1007/12-062.
4 Wu, T.; Gong, P.; Szleifer, I.; Vicek, P.; Subr, V.; Genzer, J. Behavior of surface-anchored poly(acrylic acid) brushes with grafting density gradients on solid substrates: 1. Experiment. *Macromolecules* **2007**, *40*, 8756–8764.
5 Witte, K. N.; Kim, S.; Won, Y. Y. J. Self-consistent field theory study of the effect of grafting density on the height of a weak polyelectrolyte brush. *J. Phys. Chem. B* **2009**, *113*, 11076–11084.
6 Napper, Donald H. *Polymeric stabilization of colloidal dispersions*. Academic Press, London. **1983**, Vol. 7.
7 Klein, J.; Kamiyama, Y.; Yoshizawa, H.; Israelachvili, J. N.; Fredrickson, G. H.; Pincus, P.; Fetters, L. J. Lubrication forces between surfaces bearing polymer brushes. *Macromolecules* **1993**, *26*, 5552–5560.
8 Sokoloff, J. B. Theory of the observed ultralow friction between sliding polyelectrolyte brushes. *J. Chem. Phys.* **2008**, *129*, 014901.
9 Ouyang, H.; Xia, Z. H.; Zhe, J. Voltage-controlled flow regulating in nanofluidic channels with charged polymer brushes. *Microfluid Nanofluid.* **2010**, *9*, 915–922.
10 Roy, I.; Gupta, M. N. Smart polymeric materials: emerging biochemical applications. *Chem. Biol.* **2003**, *10*, 1161–1171.
11 Patwary, J.; Chen, G.; Das, S. Efficient electrochemomechanical energy conversion in nanochannels grafted with polyelectrolyte layers with pH-dependent charge density. *Microfluid Nanofluid.* **2016**, *20*, 37.
12 Chen, G.; Das, S. J. Electroosmotic transport in polyelectrolyte-grafted nanochannels with pH-dependent charge density. *Appl. Phys.* **2015**, *117*, 185304.
13 Pincus, P. Colloid stabilization with grafted polyelectrolytes. *Macromolecules* **1991**, *24*, 2912–2919.
14 Borisov, O. V.; Zhulina, E. B.; Birshtein, T. M. Diagram of the states of a grafted polyelectrolyte layer. *Macromolecules* **1994**, *27*, 4795–4803.
15 Netz, R. R.; Andelman, D. Neutral and charged polymers at interfaces. *Phys. Rep.* **2003**, *380*, 1–95.
16 Israëls, R.; Leermakers, F. A. M.; Fleer, G. J.; Zhulina, E. B. Charged polymeric brushes: structure and scaling relations. *Macromolecules* **1994**, *27*, 3249–3261.
17 Zhulina, E. B.; Wolterink, J. K.; Borisov, O. V. Screening effects in a polyelectrolyte brush: self-consistent-field theory. *Macromolecules* **2000**, *33*, 4945–4953.
18 Csajka, F. S.; Seidel, C. Strongly charged polyelectrolyte brushes: a molecular dynamics study. *Macromolecules* **2000**, *33*, 2728–2739.
19 Seidel, C. Strongly stretched polyelectrolyte brushes. *Macromolecules* **2003**, *36*, 2536–2543.
20 Meng, D.; Wang, Q. Stimuli-response of charged diblock copolymer brushes. *J. Chem. Phys.* **2011**, *135*, 224904.
21 Hehmeyer, O. J.; Stevens, M. J. Molecular dynamics simulations of grafted polyelectrolytes on two apposing walls. *J. Chem. Phys.* **2005**, *122*, 134909.
22 Kumar, N. A.; Seidel, C. Interaction between two polyelectrolyte brushes. *Phys. Rev. E* **2007**, *76*, 02080.
23 Wynveen, A.; Likos, C. N. Interactions between planar stiff polyelectrolyte brushes. *Phys. Rev. E* **2009**, *80*, 010801.
24 Linse, P. Interaction between colloids with grafted diblock polyampholytes. *J. Chem. Phys.* **2007**, *126*, 114903.
25 Russano, D.; Carrillo, J. M. Y.; Dobrynin, A. V. Interaction between brush layers of bottle-brush polyelectrolytes: molecular dynamics simulations. *Langmuir* **2011**, *27*, 11044–11051.
26 Sjöström, L.; Akesson, T.; Jönsson, B. J. Interaction and conformation of polyelectrolyte chains adsorbed on neutral surfaces. *J. Chem. Phys.* **1993**, *99*, 4739–4747.
27 Ou, Y. P.; Sokoloff, J. B.; Stevens, M. Comparison of the kinetic friction of planar neutral and polyelectrolyte polymer brushes using molecular dynamics simulations. *J. Phys. Rev. E* **2012**, *85*, 011801.
28 He, S. Z.; Merlitz, H.; Chen, L.; Sommer, J. U.; Wu, C. X.

Polyelectrolyte brushes: MD simulation and SCF theory. *Macromolecules* **2010**, *43*, 7845−7851.
29 Malfreyt, P.; Tildesley, D. J. Dissipative particle dynamics simulations of grafted polymer chains between two walls. *Langmuir* **2000**, *16*, 4732−4740. .
30 Sirchabesan, M.; Giasson, S. Mesoscale simulations of the behavior of charged polymer brushes under normal compression and lateral shear forces. *Langmuir.* **2007**, *23*, 9713−9721.
31 Ibergay, C.; Malfreyt, P.; Tildesley, D. J. Mesoscale modeling of polyelectrolyte brushes with salt. *J. Phys. Chem. B* **2010**, *114*, 7274−7285.
32 Yang, J.; Cao, D. P. Counterion valence-induced tunnel formation in a system of polyelectrolyte brushes grafted on two apposing walls. *J. Phys. Chem. B* **2009**, *113*, 11625−11631.
33 Abraham, T.; Giasson, S.; Gohy, J. F.; Jérome, R. Direct measurements of interactions between hydrophobically anchored strongly charged polyelectrolyte brushes. *Langmuir* **2000**, *16*, 4286−4292.
34 Balastre, M.; Li, F.; Schorr, P.; Yang, J.; Mays, J. W.; Tirrell, M. V. A study of polyelectrolyte brushes formed from adsorption of amphiphilic diblock copolymers using the surface forces apparatus. *Macromolecules* **2002**, *35*, 9480−9486.
35 Raviv, U.; Giasson, S.; Kampf, N.; Gohy, J. F.; Jérome, R.; Klein, J. Lubrication by charged polymers. *Nature* **2003**, *425*, 163−165.
36 Hayashi, S.; Abe, T.; Higashi, N.; Niwa, M.; Kurihara, K. Polyelectrolyte brush layers studied by surface forces measurement: dependence on pH and salt concentrations and scaling. *Langmuir* **2002**, *18*, 3932−3944.
37 Romet-Lemonne, G.; Daillant, J.; Guenoun, P.; Yang, J.; Mays, J. W. Thickness and density profiles of polyelectrolyte brushes: dependence on grafting density and salt concentration. *Phys. Rev. Lett.* **2004**, *93*, 148301.
38 Ahrens, H.; Förster, S.; Helm, C. A. Charged polymer brushes: counterion incorporation and scaling relations. *Phys. Rev. Lett.* **1998**, *81*, 4172−4175.
39 Weir, M. P.; Heriot, S. Y.; Martin, S. J.; Parnell,A. J.; Holt, S. A.; Webster, J. R. P.; Jones, R. A. L. Voltage-induced swelling and deswelling of weak polybase brushes. *Langmuir* **2011**, *27*, 11000−11007.
40 Liu, G. Q.; Cai, M. R.; Zhou, F.; Liu, W. M. Charged polymer brushes-grafted hollow silica nanoparticles as a novel promising material for simultaneous joint lubrication and treatment. *J. Phys. Chem. B* **2014**, *118*, 4920−4931.
41 Li, B.; Yu, B.; Wang, X. L.; Guo, F.; Zhou, F. Correlation between conformation change of polyelectrolyte brushes and lubrication. *Chinese J. Polym. Sci.* **2015**, *33*, 163−172.
42 Wang, C. S.; Xie, R. J.; Liu, S.; Giasson, S. Tribological behavior of surface-immobilized novel biomimicking multihierarchical polymers: the role of structure and surface attachment. *Langmuir* **2019**, *35*, 15592−15604.
43 Zhulina, E. B.; Rubinstein, M. Lubrication by polyelectrolyte brushes. *Macromolecules* **2014**, *47*, 5825−5838.
44 Lin, W. F.; Klein, J. Recent progress in cartilage lubrication. *Adv. Mater.* **2021**, *33*, 2005513.
45 Adibnia, V.; Mirbagheri, M.; Faivre, J.; Robert, J.; Lee, J.; Matyjaszewski, K.; Lee. D. W.; Banquy, X. Bioinspired polymers for lubrication and wear resistance. *Prog. Polym. Sci.* **2020**, *110*, 101298.
46 Jahn, S.; Seror, J.; Klein, J. Annu. Rev. Lubrication of Articular Cartilage. *Biomed. Eng.* **2016**, *18*, 235−258.
47 Lin, W. F.; Klein, J. Direct measurement of surface forces: recent advances and insights. *Appl. Phys. Rev.* **2021**, *8*, 031316.
48 Lin, W. F.; Klein, J. Control of surface forces through hydrated boundary layers. *Curr. Opin. in Colloid Interface Sci.* **2019**, *44*, 94−106.
49 Grest, G. S. Interfacial sliding of polymer brushes: a molecular dynamics simulation. *Phys. Rev. Lett.* **1996**, *76*, 4979−4982.
50 Murat, M.; Grest, G. S. Interaction between grafted polymeric brushes: a molecular-dynamics study. *Phys. Rev. Lett.* **1989**, *63*, 1074−1077.
51 Kreer, T.; Müser, M. H.; Binder, K.; Klein, J. Frictional drag mechanisms between polymer-bearing surfaces. *Langmuir* **2001**, *17*, 7804−7813.
52 Sandberg, D. J.; Carrillo, J. M. Y.; Dobrynin, A. V. Molecular dynamics simulations of polyelectrolyte brushes: from single chains to bundles of chains. *Langmuir* **2007**, *23*, 12716−12728.
53 Cao, Q.; Zuo, C.; He, H. Shearing and compression behavior of end-grafted polyelectrolyte brushes with mono- and trivalent counterions: a molecular dynamics simulation. *Modell. Simul. Mater. Sci. Eng.* **2010**, *18*, 7.
54 Liberelle, B.; Giasson, S. Friction and normal interaction forces between irreversibly attached weakly charged polymer brushes. *Langmuir.* **2008**, *24*, 1550−1559.
55 Goujon, F.; Malfreyt, P.; Tildesley, D. Dissipative particle dynamics simulations in the grand canonical ensemble: applications to polymer brushes. *Chem. Phys. Chem.* **2004**, *5*, 457−464.
56 Raviv, U.; Klein, J. Fluidity of Bound Hydration Layers. *Science* **2002**, *297*, 1540−1543.
57 Raviv, U.; Giasson, S.; Kampf, N.; Gohy, J. F.; Jerome, R.; Klein, J. Normal and frictional forces between surfaces bearing polyelectrolyte brushes. *Langmuir* **2008**, *24*, 8678−8687.
58 Duan, M. Y.; Chen, G. Swelling and shrinking of two opposing polyelectrolyte brushes. *Phys. Rev. E* **2023**, DOI: 10.1103/PhysRevE.107.024502.
59 Witte, K. N.; Won, Y. Y. Self-consistent-field analysis of mixed polyelectrolyte and neutral polymer brushes. *Macromolecules* **2006**, *39*, 7757−7768.
60 Shi, A. C.; Noolandi, J. Theory of inhomogeneous weakly charged polyelectrolytes. *Macromol. Theory Simul.* **1999**, *8*, 214−229.
61 Wang, Q.; Taniguchi, T.; Fredrickson, G. H. Self-consistent field theory of polyelectrolyte systems. *J. Phys. Chem. B* **2004**, *108*, 6733−6744.
62 Lewis, T.; Ganesan, V. Mean-field modeling of the encapsulation of weakly acidic molecules in polyelectrolyte dendrimers. *J. Phys. Chem. B* **2012**, *116*, 8269−8281.
63 Kumar, R.; Sumpter. B. G.; Kilbey II, S. M. Charge regulation and local dielectric function in planar polyelectrolyte brushes. *J. Chem. Phys.* **2012**, *136*, 234901.
64 Gong, P.; Genzer, J.; Szleifer, I. Phase behavior and charge regulation of weak polyelectrolyte grafted layers. *Phys. Rev. Lett.* **2007**, *98*, 018302.
65 Kim J. U.; Masten, M. W. Interaction between polymer-grafted particles. *Macromolecules* **2008**, *41*, 4435−4443;
66 Kim, J. U.; Masten, M. W. Repulsion exerted on a spherical particle by a polymer brush. *Macromolecules* **2008**, *41*, 246−252.
67 Manning, G. S. Limiting laws and counterion condensation in polyelectrolyte solutions I. Colligative properties. *J. Chem. Phys.* **1969**, *51*, 924−933.
68 Wang, M. L.; Tong, C. A numerical study of two opposing polyelectrolyte brushes by the self-consistent field theory. *RSC Adv.* **2014**, *4*, 20769−20780.